Study of Chemical and Morphological Transformations during Ni$_2$Mo$_3$N Synthesis via an Oxide Precursor Nitration Route

Denis V. Leybo [1],* , **Dmitry I. Arkhipov [1]**, **Konstantin L. Firestein [2]** and **Denis V. Kuznetsov [1]**

[1] National University of Science and Technology "MISiS", 119049 Moscow, Russia;
   hipa2010@yandex.ru (D.I.A.); dk@misis.ru (D.V.K.)

[2] School of Chemistry, Physics and Mechanical Engineering, Science and Engineering Faculty,
   Queensland University of Technology (QUT), 2nd George st., Brisbane, QLD 4000, Australia;
   konstantin.faershteyn@qut.edu.au

* Correspondence: leybodv@gmail.com; Tel.: +7-499-237-2226

Abstract: Chemical and morphological transformations during Ni$_2$Mo$_3$N synthesis were studied in this work. Nitride samples were synthesized from oxide precursors in H$_2$/N$_2$ flow and were analyzed by thermogravimetry, X-ray diffraction analysis, scanning electron microscopy, and energy dispersive X-ray spectroscopy methods. In addition, physical and chemical adsorption properties were studied using low-temperature N$_2$ physisorption and NH$_3$ temperature-programmed desorption. It was shown that nitride formation proceeds through a sequence of phase transformations: NiMoO$_4$ + MoO$_3$ → Ni + NiMo + MoO$_2$ → Ni + NiMo + Mo$_2$N → Ni$_2$Mo$_3$N. The weight changes that were calculated from the proposed reactions were in agreement with the experimental data from thermogravimetry. The morphology of the powder changed from platelets and spheres for the oxide sample, to aggregates of needle-like particles for the intermediate product, to porous particles with an extended surface area for the nitride final product. The obtained results should prove useful for subsequent Ni$_2$Mo$_3$N based catalysts production process optimization.
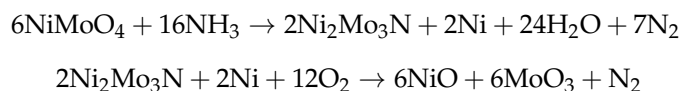
Keywords: Ni$_2$Mo$_3$N; Ni-Mo nitride; chemical transformations; thermogravimetry

1. Introduction

The global industry demand for novel highly active and selective hydrogenation catalysts has stimulated research into the synthesis and characterization of materials presenting potential for industrial applications. One class of such materials is the transition metal nitrides. Binary molybdenum nitrides possess catalytic activity in hydrogen-mediated reactions such as ammonia synthesis, NO reduction, hydrogenation of CO, and ethyne [1]. The addition of nickel to produce ternary nitrides can be useful to further improve the catalytic properties of molybdenum nitride. Recently it was shown by our group that Ni-Mo nitride could be used as a catalyst for CO$_x$-free hydrogen production via ammonia decomposition for low-temperature hydrogen fuel cell applications [2].

Ni$_2$Mo$_3$N nitride can be synthesized through different routes, including the ammonolysis of oxide precursors [3], the decomposition of complex organometallic salts in inert atmosphere [4], the reduction of nitrogen-containing inorganic salts in hydrogen [5], and the nitration of metastable precursors [6]. Recently, new a method for the synthesis of Ni$_2$Mo$_3$N phase using citric acid as a chelating agent was developed by Zaman et al. [7]. All of the methods involved the incorporation of nitrogen into the lattice of Ni-Mo from either the gas phase or the solid precursor. However, the chemical transformations that occurred during the synthesis of nitrides were not studied extensively. Herle et al. [8] studied the oxidation process of the nitride Ni$_2$Mo$_3$N by means of a quadrupole mass-spectrometer and

suggested that the process of nitride formation by ammonolysis and its oxidation proceed according to these reactions:

$$6NiMoO_4 + 16NH_3 \rightarrow 2Ni_2Mo_3N + 2Ni + 24H_2O + 7N_2$$

$$2Ni_2Mo_3N + 2Ni + 12O_2 \rightarrow 6NiO + 6MoO_3 + N_2$$

However, the final product contained Ni metal impurity and the ammonolysis process was not studied in detail with consideration of phase transformations during synthesis. Wang et al. [6] have shown that the formation of nitride is possible from Ni metal and binary nitride Mo_2N. This indirectly suggested that the formation of ternary nitride proceeds through the formation of the binary nitride step.

Although there are several works which mention possible routes of phase transformations in the Ni-Mo-N system during the synthesis of nitride, there is no, to the best of our knowledge, comprehensive study of these phenomena. The main reason is that most of the nitride production methods include the application of complex precursors, in which phase composition is hard to identify. In this respect, simplification is needed. Mixed oxide precursors are appropriate model systems since, even in the case of complex salts, we can expect that high-temperature transformations will be similar. The morphology of the nitride products strongly affects the properties of the catalysts. Thus, it is essential to understand the changes of the particles structure during Ni-Mo nitride formation.

The study of chemical and morphological transformations can help improve the methods for the production of nitrides with controllable properties. The aim of this work is to elucidate these transformations during the synthesis of Ni-Mo nitride from oxide precursors.

2. Results

2.1. Thermogravimetry Analysis Results

The results of the thermogravimetric analysis are presented in Figure 1. From this graph, one can see that the reduction process proceeded in two steps with two maxima in weight rate changes at 495 °C and 705 °C. The arrows in Figure 1 indicate the temperatures at which the reduction process was interrupted in order to study the phase and the morphology changes. The weight changes during each step are also shown in the graph.
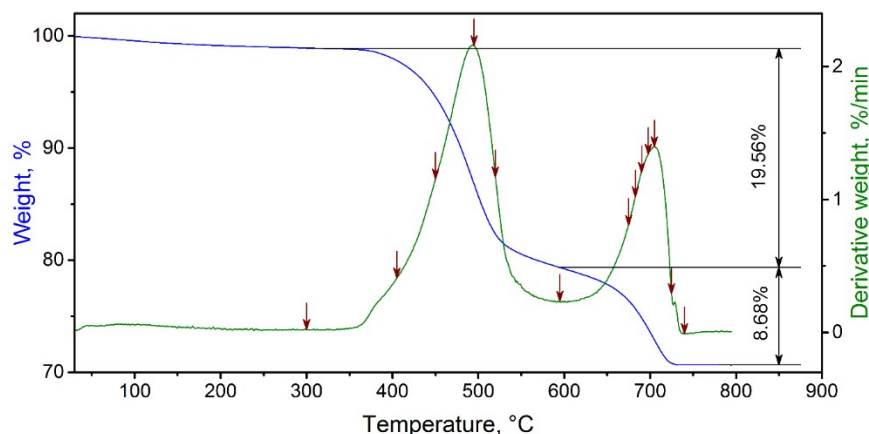

Figure 1. Thermogravimetric results for the oxide precursor in 100 mL/min 20% N_2/H_2 flow. Heating rate of 10 °C/min. Arrows indicate temperatures at which the process was interrupted in order to study chemical and morphological transformations.

2.2. XRD Analysis Results

Figure 2 shows XRD patterns of samples reduced at different temperatures. Initially, the oxide sample consists of two phases: MoO_3 and $NiMoO_4$ (PDF cards no. 00-005-0508 and 01-086-0361

respectively). At 405 °C, the intensity of the peaks corresponding to the $NiMoO_4$ phase started to decrease. The peak of MoO_2 (PDF card no. 03-065-1273) at 39.24° appeared at 450 °C. Further, the intensity of the peak around 67° increased and its shape broadened. This may indicate the formation of the Ni and NiMo phases (PDF cards no. 03-065-0380 and 03-065-6903 respectively). At 520 °C, peaks of MoO_2, Ni and NiMo phases could be clearly identified and, at 595 °C, the specimen contained only these three phases. This temperature corresponds to the local minimum of the weight change rate on the thermogravimetric curve, and the specimen at 595 °C can be considered as an intermediate product of Ni_2Mo_3N formation. A broad peak around 57° appeared on the XRD pattern of the sample treated at 675 °C. The peak corresponds to the Mo_2N phase (PDF card no. 01-075-1150), which was present in the samples up to 750 °C. The Ni_2Mo_3N phase peaks (PDF card no. 01-089-4564) appeared at 683 °C. The intensity of the Ni_2Mo_3N phase peaks increased until 750 °C, while the intensity of Mo_2N, MoO_2, NiMo, and Ni peaks decreased. The final sample treated at 750 °C consisted of about 92 wt.% of Ni_2Mo_3N, and 4 wt.% of Mo_2N and NiMo.
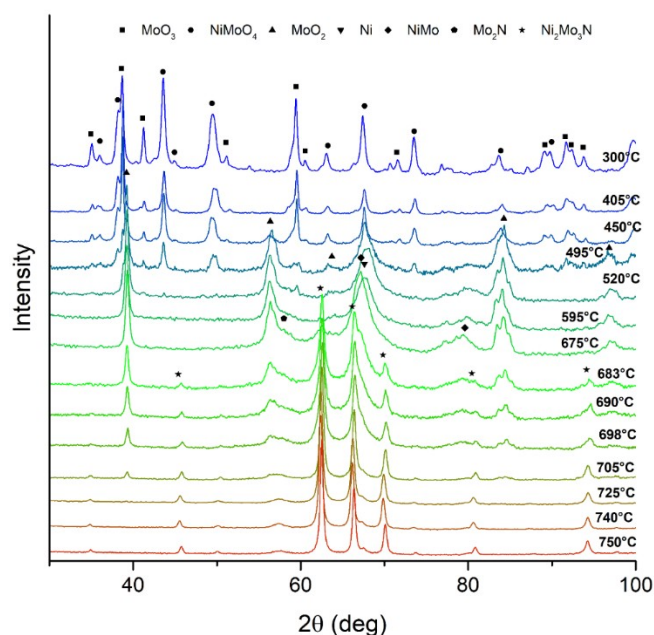

Figure 2. XRD patterns of samples heated to different temperatures in 100 mL/min 20% N_2/H_2 flow.

2.3. SEM Analysis Results

Figure 3 shows micrograph of samples heat-treated at 300, 595 and 750 °C corresponding to minima of the weight vs. temperature thermogravimetric plot. We may see from Figure 3 that the sample at 300 °C consisted of two types of particles: Platelet-shaped particles with sizes from 5 to 10 μm, and nanosized particles either isolated or aggregated. At 595 °C one may also observe two different types of morphology (Figure 4): The aggregates of needle-like particles, and the needle-like particles incorporated into aggregates of larger particles. It was hard to differentiate between the particles according to morphology for the high-temperature specimen (Figure 5). The final product consisted of particles with a highly porous structure.
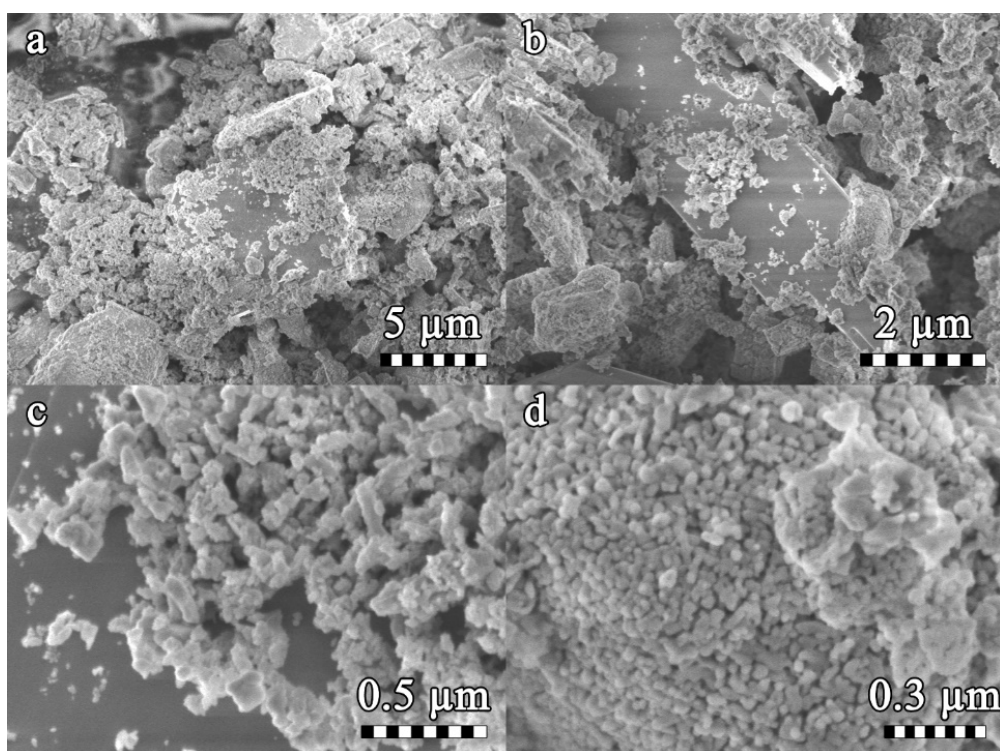
Figure 3. SEM images of sample heat-treated at 300 °C in 100 mL/min 20% N_2/H_2 flow. Magnification: (**a**) ×7200; (**b**) ×21,000; (**c**) ×84,000; (**d**) ×117,000
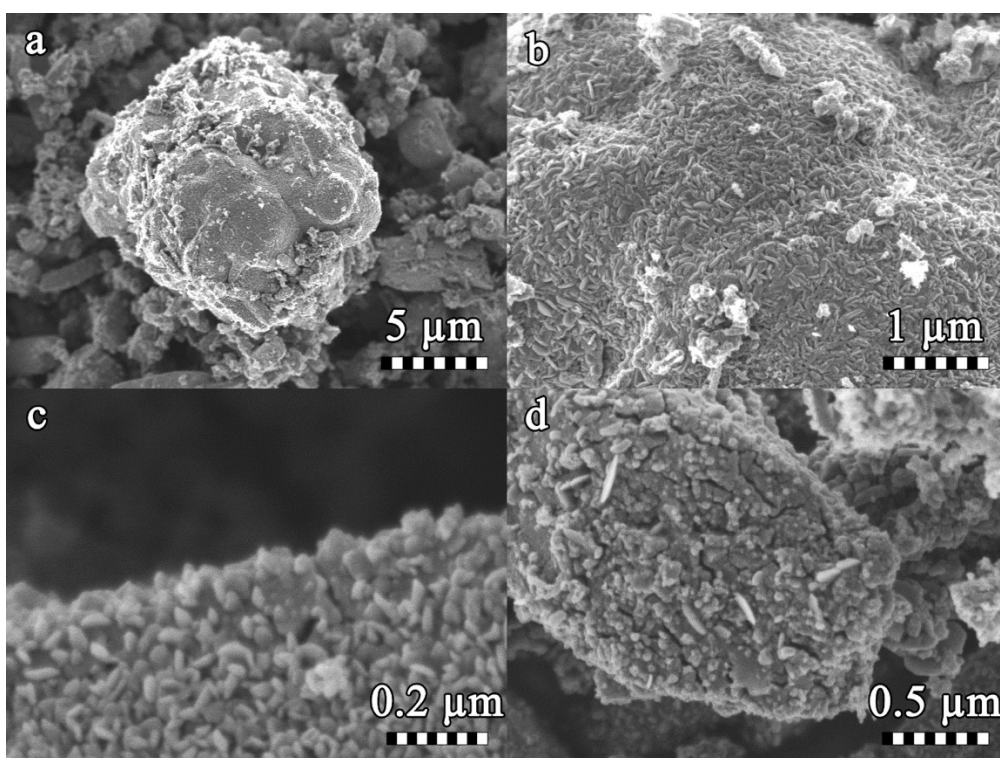
Figure 4. SEM images of sample heat-treated at 595 °C in 100 mL/min 20% N_2/H_2 flow. Magnification: (**a**) ×7200 (**b**) ×36,000 (**c**) ×170,000 (**d**) ×72,000
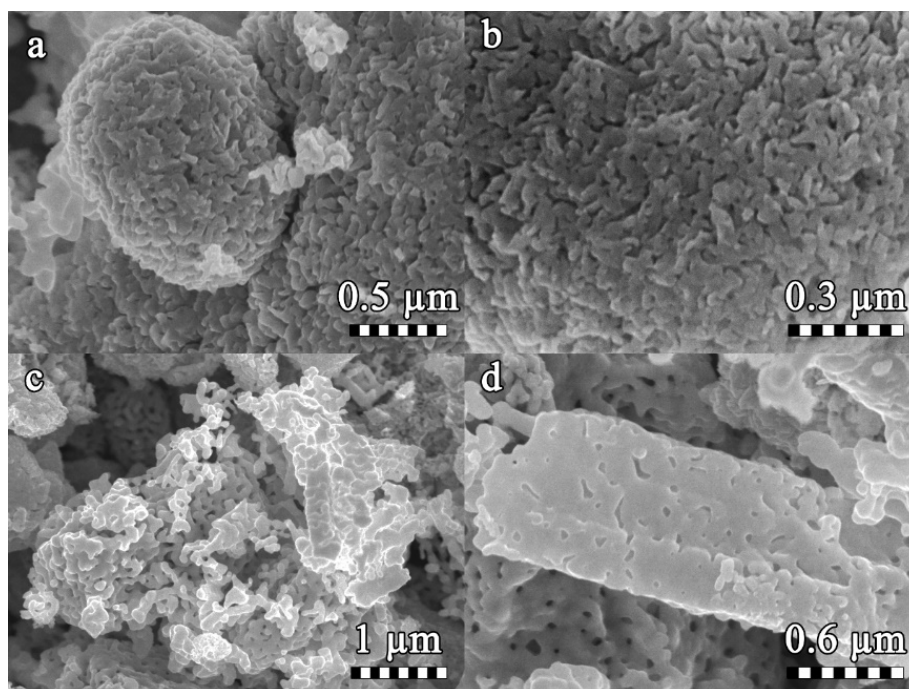
Figure 5. SEM images of sample heat-treated at 740 °C in 100 mL/min 20% N_2/H_2 flow. Magnification: (**a**) ×72,000 (**b**) ×143,000 (**c**) ×36,000 (**d**) ×72,000

2.4. Adsorption Analysis Results

In order to gain more insight into the functional properties of the Ni_2Mo_3N phase, adsorption studies were done on a sample heat-treated in a H_2/N_2 gas mixture at 650 °C. The results of low-temperature N_2 physisorption are shown on Figure 6.
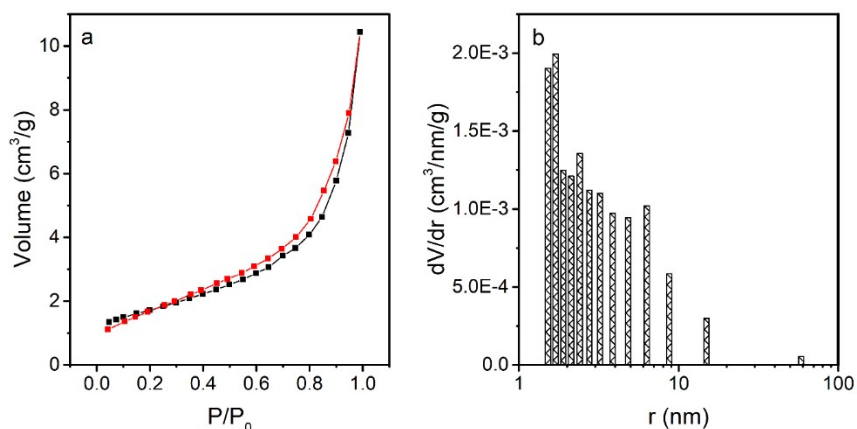

Figure 6. Low-temperature N_2 adsorption study results for a Ni_2Mo_3N sample heat-treated in H_2/N_2 atmosphere at 650 °C. (**a**) Adsorption (black) and desorption (red) isotherms; (**b**) pore-size distribution calculated by means of the BJH method.

The obtained isotherm corresponds to an IV type isotherm [9], characteristic of mesoporous samples with a H3 type hysteresis loop (Figure 6a). Pore-size distribution shows that the maximum volume of the pores has size below 2 nm (Figure 6b). The specific surface area, calculated from isotherm by BET equation, equaled 6.1 m^2/g, while mean pore size was 1.7 nm with a total pore volume of 0.015 cm^3/g.

The results of the TPD-NH$_3$ experiment are shown on Figure 7. The desorption profiles of ammonia (m/z = 16), hydrogen (m/z = 2) and nitrogen (m/z = 28) were recorded during the experiment.

One can see on Figure 7 that there is a sharp peak of ammonia with a maximum at 195 °C, which corresponds to the desorption of the unreacted chemically adsorbed ammonia. The peaks on the desorption profiles of the hydrogen and nitrogen indicate that the ammonia decomposes on the surface of the nitride. It can be seen that hydrogen desorption happened in two steps, with peak maxima at 630 and 840 °C. The desorption of nitrogen also proceeds in two steps, with a sharp peak at 525 °C and wide peak at 790 °C. The high-temperature peak of the nitrogen desorption profile could be ascribed to the decomposition of the nitride, as was noted in Reference [10].
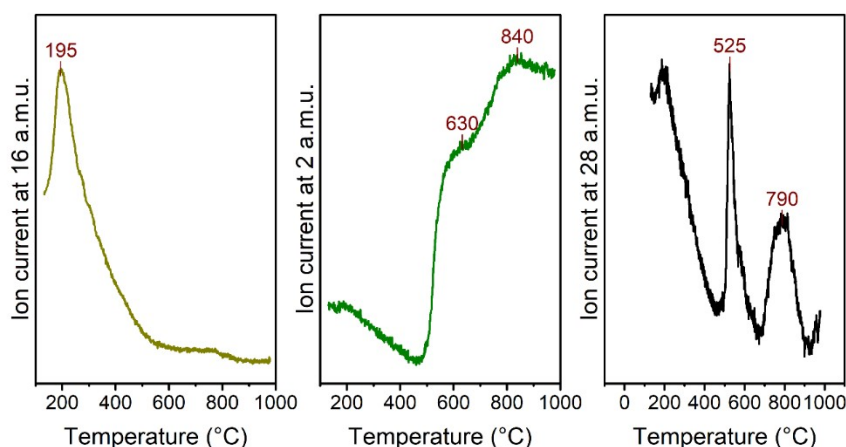

Figure 7. NH_3 TPD results of a Ni_2Mo_3N sample heat-treated in a H_2/N_2 atmosphere at 650 °C.

3. Discussion

On the basis of the XRD analysis of the samples treated at different temperatures, we can write the reactions occurring during each step of Ni_2Mo_3N formation. During the first stage, MoO_3 and $NiMoO_4$ oxides are reduced to MoO_2, Ni and NiMo according to the reaction:

$$2NiMoO_4 + MoO_3 + 7H_2 \rightarrow 2MoO_2 + Ni + NiMo + 7H_2O \tag{1}$$

A second step involves the formation of a Mo_2N phase from MoO_2 and the reaction of Ni with molybdenum nitride form Ni_2Mo_3N according to the relations:

$$2MoO_2 + \frac{1}{2}N_2 + 4H_2 \rightarrow Mo_2N + 4H_2O \tag{2}$$

$$Mo_2N + Ni + NiMo \rightarrow Ni_2Mo_3N. \tag{3}$$
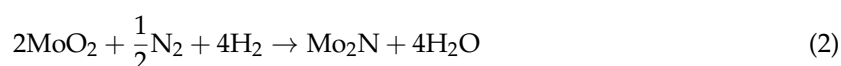
The overall reaction of Ni_2Mo_3N formation from the oxide precursor can be written as:

$$2NiMoO_4 + MoO_3 + \frac{1}{2}N_2 + 11H_2 \rightarrow Ni_2Mo_3N + 11H_2O \tag{4}$$
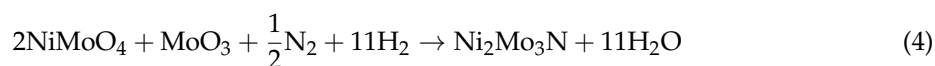
In Table 1 we present the comparison of weight changes corresponding to the reactions with the results of the thermogravimetric data. The calculated data are in good agreement with the experimental results. The small discrepancy can be explained by the fact that the final product does not consist of 100 wt.% of Ni_2Mo_3N. The low-temperature weight loss on the thermogravimetric curve can be ascribed to the water evolution during the dehydration of $NiMoO_4 \cdot xH_2O$.

Table 1. Comparison of weight changes calculated from Equations (1)–(3) with the experimental values obtained from thermogravimetric analysis.

Temperature Range of Step, °C	Experimental, %	Calculated, %
300–595	19.56	19.27
595–750	8.68	8.60

In order to reveal the changes in morphology that accompany Ni-Mo nitride production, a SEM analysis of samples that were heat-treated at 300, 595 and 750 °C was completed. The shape of the larger particles in the sample that was heat-treated at 300 °C (Figure 3) suggests that we were in the presence of MoO_3, which crystallizes in the anisotropic orthorhombic structure. EDX analysis of these particles showed that these regions are poor in nickel, which confirms this suggestion. The Ni/Mo ratio in the little particle aggregates was close to one which, taking into account XRD results, corresponds to the $NiMoO_4$ particles. The EDX analysis of the sample that was heat-treated at 595 °C (Figure 4) showed that the aggregates of the needle-like particles were very poor in nickel. Considering the phase transformations mentioned above, we can conclude that the needle-like particle aggregates consist of MoO_2 reduced from MoO_3. The second type of particles consist of needle-like MoO_2 incorporated into the bigger Ni and NiMo particles. The high-temperature specimen is homogeneous in morphology and consists of only porous Ni_2Mo_3N particles. Thus, from the SEM results we can conclude that, at least up to 595 °C, there is inhomogeneity in the composition throughout the sample and that mixing of the powder during the reduction process should be considered.

4. Materials and Methods

All samples studied in this work were produced using methods previously described in the literature [11]. In short, $Ni(CH_3COO)_2 \cdot 4H_2O$ was dissolved in distilled water, and $(NH_4)_6Mo_7O_{24} \cdot 4H_2O$ was dissolved in 25 wt. % ammonia hydroxide solution. The amount of salt was calculated in order to obtain a Ni/Mo ratio equal to 2/3. The solutions were mixed and evaporated to dryness. The obtained mixed salt was dried at 95 °C overnight and subsequently calcined at 500 °C for 4 h. The oxide precursor that was produced in this way was reduced at different temperatures on a thermogravimetric analyzer in 100 mL/min 20% N_2/H_2 flow. The analyzer was programed to heat the sample at 10 °C/min to the desired temperature and then immediately forced to cool to room temperature. After cooling the sample, the gas flow was changed to 1% O_2/N_2 mixture in order to prevent the bulk oxidation of the reduced sample upon exposure to air. The samples were then studied by X-ray diffraction (XRD) and scanning electron microscopy (SEM).

Thermogravimetric analysis of the oxide precursor was performed on an SDT Q600 instrument (TA Instruments, New Castle, DE. USA). The sample was heated at the rate of 10 °C/min to 800 °C in 100 mL/min 20% N_2/H_2 flow.

XRD patterns were obtained on a Difrey-401 powder diffractometer (Scientific Instruments, St. Petersburg, Russia) equipped with a position sensitive detector capable of simultaneous spectrum collection in the Δ2θ range of 58°. Spectra were measured at room temperature with Cr-K$_\alpha$ radiation (λ = 2.2909 Å) in the 2θ range of 30–100°, with 300 s exposition at each detector position. The phase content was estimated using the reference intensity ratio method.

The morphology of the particles, as well as the elemental composition, were studied by SEM and energy dispersive X-Ray spectroscopy (EDX) on a JSM-7600F (Jeol Ltd., Tokyo, Japan) equipped with an 80 mm^2 X-Max EDX detector (Oxford Instruments, Abingdon, UK). The microphotographs were obtained in secondary electrons with an accelerating voltage of 10 kV.

The low-temperature N_2 adsorption for the nitride sample heat-treated at 650 °C in N_2/H_2 atmosphere was done on a Nova 1200e instrument (Quantachrome Instruments, Boynton Beach, FL, USA). Prior to the adsorption experiment, approximately 200 mg of the sample was firstly degassed in a vacuum at 120 °C overnight. The adsorption was performed at 77 K. The specific surface area was

calculated using the Brunauer-Emmett-Teller (BET) method. Pore size distribution was obtained by means of the Barrett-Joyner-Halenda (BJH) method using the desorption branch of the isotherm.

The NH_3 temperature programmed desorption (TPD-NH_3) experiments were performed using ChemBET Pulsar equipment (Quantachrome Instruments, Boynton Beach, FL, USA). In the experiment, approximately 100 mg of the sample that was diluted with quartz granules was loaded into a U-shaped quartz tube. Prior to the desorption experiment, the specimen was subjected to heat treatment in 3.5 mL/min N_2/14 mL/min H_2 at 650 °C for 30 min. Then gas flow was changed to 30 mL/min of He and held at 650 °C for another 30 min. Adsorption of ammonia was performed at 130 °C with 14 mL/min flow of pure ammonia gas for 30 min following a purge with 30 mL/min of He for another 30 min. TPD was done in 30 mL/min He flow in linear heating mode with a 10°/min heating rate up to 1000 °C.

5. Conclusions

Chemical transformations and morphology changes during the production of Ni_2Mo_3N were studied in this work. XRD and thermogravimetric analyses of samples during the nitration of oxide precursors in N_2/H_2 flow demonstrates that the formation proceeds through the sequence: $NiMoO_4 + MoO_3 \rightarrow Ni + NiMo + MoO_2 \rightarrow Ni + NiMo + Mo_2N \rightarrow Ni_2Mo_3N$. The morphology of the powder changes from platelets and spheres for the oxide sample, to aggregates of needle-like particles for the intermediate product, to porous particles with an extended surface area for the nitride final product. It was shown that there is inhomogeneity in the composition throughout the sample at least up to 595 °C, and that mixing of the powder during the reduction process should be considered. The obtained results are useful for subsequent Ni_2Mo_3N based catalyst production process optimization.

Author Contributions: Investigation, D.V.L.; methodology, D.V.L., D.I.A. and K.L.F.; project administration, D.V.K.; and writing—original draft, D.V.L.

Conflicts of Interest: The authors declare no conflicts of interest.

References

1. Cardenas-Lizana, F.; Lamey, D.; Gomez-Quero, S.; Perret, N.; Kiwi-Minsker, L.; Keane, M.A. Selective three-phase hydrogenation of aromatic nitro-compounds over β-molybdenum nitride. *Catal. Today* **2011**, *173*, 53–61. [CrossRef]
2. Leybo, D.V.; Baiguzhina, A.N.; Muratov, D.S.; Arkhipov, D.I.; Kolesnikov, E.A.; Levina, V.V.; Kosova, N.I.; Kuznetsov, D.V. Effects of composition and production route on structure and catalytic activity for ammonia decomposition reaction of ternary Ni-Mo nitride catalysts. *Int. J. Hydrogen Energy* **2016**, *41*, 3854–3860. [CrossRef]
3. Villasana, Y.; Escalante, Y.; Nuñez, J.E.R.; Méndez, F.J.; Ramírez, S.; Luis-Luis, M.Á.; Cañizales, E.; Ancheyta, J.; Brito, J.L. Maya crude oil hydrotreating reaction in a batch reactor using alumina-supported NiMo carbide and nitride as catalysts. *Catal. Today* **2014**, *220–222*, 318–326. [CrossRef]
4. Chouzier, S.; Vrinat, M.; Cseri, T.; Roy-Auberger, M.; Afanasiev, P. HDS and HDN activity of (Ni,Co)Mo binary and ternary nitrides prepared by decomposition of hexamethylenetetramine complexes. *Appl. Catal. A Gen.* **2011**, *400*, 82–90. [CrossRef]
5. Wang, Z.-Q.; Ma, Y.-L.; Zhang, M.-H.; Li, W.; Tao, K. A novel route to the synthesis of bulk and well dispersed alumina-supported Ni_2Mo_3N catalysts via single-step hydrogen thermal treatment. *J. Mater. Chem.* **2008**, *18*, 4421–4425. [CrossRef]
6. Wang, H.; Wu, Z.; Kong, J.; Wang, Z.; Zhang, M. Synthesis of transition metal nitride by nitridation of metastable oxide precursor. *J. Solid State Chem.* **2012**, *194*, 238–244. [CrossRef]
7. Zaman, S.F.; Jolaoso, L.A.; Podila, S.; Al-Zahrani, A.A.; Alhamed, Y.A.; Driss, H.; Daous, M.M.; Petrov, L. Ammonia decomposition over citric acid chelated γ-Mo_2N and Ni_2Mo_3N catalysts. *Int. J. Hydrogen Energy* **2018**, *43*, 17252–17258. [CrossRef]

8. Herle, P.S.; Hegde, M.S.; Sooryanarayana, K.; Row, T.N.G.; Subbanna, G.N. Ni$_2$Mo$_3$N: A new ternary interstitial nitride with a filled β-manganese structure. *Inorg. Chem.* **1998**, *37*, 4128–4130. [CrossRef] [PubMed]

9. ALOthman, Z.A. A Review: Fundamental Aspects of Silicate Mesoporous Materials. *Materials* **2012**, *5*, 2874–2902. [CrossRef]

10. Srifa, A.; Okura, K.; Okanishi, T.; Muroyama, H.; Matsui, T.; Eguchi, K. CO$_x$-free hydrogen production via ammonia decomposition over molybdenum nitride-based catalysts. *Catal. Sci. Technol.* **2016**, *6*, 7495–7504. [CrossRef]

11. Fan, X.; Zhang, H.; Li, J.; Zhao, Z.; Xu, C.; Liu, J.; Duan, A.; Jiang, G.; Wei, Y. Ni-Mo nitride catalysts: Synthesis and application in the ammoxidation of propane. *Chin. J. Catal.* **2014**, *35*, 286–293. [CrossRef]